Scripta Materialia 195 (2021) 113694

Contents lists available at ScienceDirect

Scripta Materialia

journal homepage: www.elsevier.com/locate/scriptamat

# Formation of $\{11\bar{2}2\}$ contraction twins in titanium through reversible martensitic phase transformation

Amir Hassan Zahiri[1], Jamie Ombogo[1], Lei Cao*

*Department of Mechanical Engineering, University of Nevada, Reno, NV 89557, USA*

ARTICLE INFO

*Article history:*
Received 19 October 2020
Revised 3 December 2020
Accepted 21 December 2020

*Keywords:*
Twinning
Titanium
Martensitic phase transformation
Omega phase
Molecular dynamics simulations

ABSTRACT

We report the discovery of a non-conventional $\{11\bar{2}2\}$ twinning mechanism in $\alpha$-titanium through reversible $\alpha \rightarrow \omega \rightarrow \alpha$ martensitic phase transformations. Specifically, the parent $\alpha$-phase first transforms into an intermediate $\omega$-phase, which then quickly transforms into a twin $\alpha$-phase, leading to the formation of $\{11\bar{2}2\}$ contraction twins. In addition, we prove that the reversible $\alpha \rightarrow \omega \rightarrow \alpha$ phase transformations follow strict orientation relations between the parent $\alpha$-, intermediate $\omega$-, and twin $\alpha$-phases. Finally, we demonstrate that our mechanism agrees with classical twinning theory in the shuffle, shear, and conjugate twinning plane. This study reveals the important role of the intermediate $\omega$-phase in the twinning process, adding critical details to the existing mechanism of $\{11\bar{2}2\}$ twinning.



Titanium (Ti) and its alloys can exhibit high strength-to-weight ratio and extraordinary high-temperature performance. Thus, they have great promise as replacements for the conventional structural materials in the automotive, aerospace, and biomedical industries [1–3]. Due to the limited number of slip systems in hcp structure, twinning plays an important role in the deformation process and mechanical properties of Ti [4,5]. Specifically, $\{10\bar{1}2\}$ and $\{11\bar{2}1\}$ are extension twins that can accommodate $\langle c\rangle$-axis extension, while $\{11\bar{2}2\}$ and $\{10\bar{1}1\}$ twins are contraction twins that can accommodate $\langle c\rangle$-axis compression. Among the contraction twins, the $\{11\bar{2}2\}$ mode dominates at temperatures below $\sim 400$ °C and, therefore, is critical to the plastic deformation of Ti at room temperature [6,7].

Rapperport determined that the experimentally observed $\{11\bar{2}2\}$ twins have the second undistorted plane $K_2 = \{11\bar{2}4\}$ and a homogeneous shear along $\eta_1 = \langle 11\bar{2}\bar{3}\rangle$, in which one third of Bravais lattice points are sheared to the perfect twin position [8,9]. Subsequently, detailed atom movements corresponding to the homogeneous shear and the shuffles of the other two thirds of Bravais lattice points were devised for various hcp materials [4,10]. Expanding on this work, Serra and Bacon detailed the interface structure and twinning dislocations for the $\{11\bar{2}2\}$ mode using molecular dynamics (MD) simulations [11,12]. Specifically, three stable interface structures were obtained for $\{11\bar{2}2\}$ twin boundaries: one with a perfect mirror symmetry and the other two with additional rigid-body translations of the twin with respect to the parent phase along the shear direction $\eta_1$. More recently, the interface energy and twinning dislocations for $\{11\bar{2}2\}$ twins were characterized by first-principles calculations [13] and classical MD simulations [14,15]. However, these studies focused on twin growth of pre-implanted $\{11\bar{2}2\}$ twin boundaries, thereby missing the formation process of the twin embryo. In a recent MD study of single-crystal Ti, Rawat and Mitra observed the nucleation of the $\{11\bar{2}2\}$ twin in Ti [16]. However, the twin was found to nucleate from an unknown structure, and the detailed nucleation process was not analyzed.

In a recent paper, we reported the formation of $\{10\bar{1}2\}$ extension twins in magnesium through reversible martensitic phase transformations with a metastable tetragonal phase as the intermediate state [17]. Unlike the rather pristine samples in previous studies [11,18,19], our carefully-designed MD simulations included a large number of initial defects, better mimicking the realistic samples used in experiments. The objective of this paper is to use MD simulations to investigate the dynamic twin formation process for $\{11\bar{2}2\}$ contraction twins in Ti, particularly focusing on the possible intermediate phase.

In this work, MD simulations are conducted using the LAMMPS package [20]. The modified embedded-atom method (MEAM) potential developed by Hennig et al. [21], which was carefully designed to capture the $\alpha \leftrightarrow \omega$ martensitic phase transformation, is used to model interatomic interactions in Ti. A time-step size of 1 fs is used to guarantee the accurate execution of the MD simulations. The periodic boundary condition is applied to all three dimensions for a one-million-atom supercell of quenched Ti, sized

* Corresponding author.
*E-mail address:* leicao@unr.edu (L. Cao).
[1] The first and second authors contributed equally.

https://doi.org/10.1016/j.scriptamat.2020.113694
1359-6462/

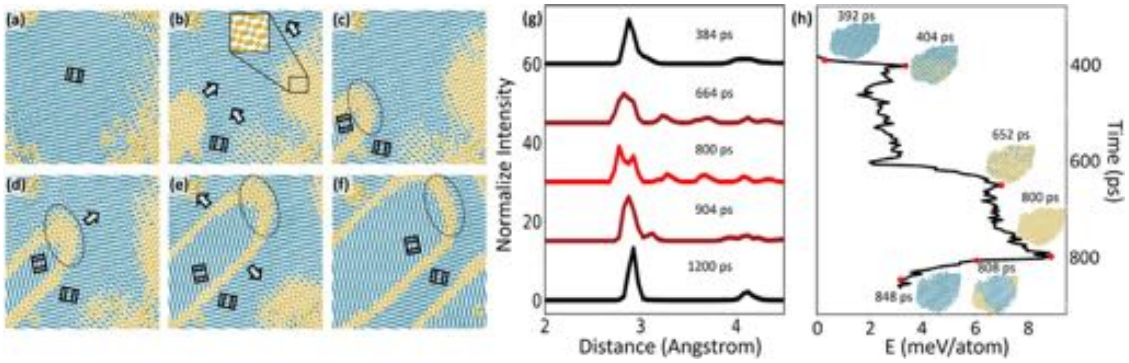


**Fig. 1.** (a–f) The microstructure evolution during the $\{11\bar{2}2\}$ twin formation process in our MD simulation, projected along the $[1\bar{1}00]_\alpha$ direction. Common neighbor analysis [29,30] is used to identify the crystal structure, with $\omega$- and $\alpha$-phases denoted in yellow and cyan, respectively. The inset in (b) shows the close-up view of the $\omega$-phase. The arrows represent the growing directions of the $\omega$-variants in (b), of the twin tip in (d), and of the twin boundaries in (e). The $\omega$-phase in the twin tip is encircled in (c)–(f). Figure 1(g) shows the evolution of the radial distribution function of a group of approximately 639 atoms and (h) shows the corresponding average potential energy during the deformation process. (For interpretation of the references to color in this figure legend, the reader is referred to the web version of this article.)

$27.4 \times 27.1 \times 23.4$ nm$^3$. The quenched Ti is obtained using the same approach as in our previous work [22,23] and is primarily $\omega$-phase (simple hexagonal), the ground state for Ti [24,25]. At the beginning of our simulations, we relax the structure at 10 K and 0 Pa in the isothermal-isobaric ensemble using the Nosé-Hoover thermostat[26] and the Parrinello-Rahman barostat[27] for 100 ps. It is then subject to z-axis compression with a strain rate of $10^8$/s and partially transforms into the $\alpha$-phase because it only has a slightly higher energy than the $\omega$-phase. OVITO [28] is used to visualize the microstructure evolution. Common neighbor analysis [29,30] is used to identify the crystal structure, with $\omega$, $\beta$, $\alpha$, and fcc phases denoted in yellow, red, cyan, and green, respectively.

Fig. 1 a–f show the microstructure evolution in our MD simulation, projected along the $[1\bar{1}00]_\alpha$ direction, which reveals the nucleation of $\{11\bar{2}2\}$ twins, followed by lengthening and thickening. At 1260 ps, the region remains in the $\alpha$-phase, as shown in Fig. 1a. With increasing strain, two $\omega$-variants nucleate and reach the maximum size at 1548 ps (Fig. 1b). Within 16 ps, the intermediate $\omega$-phase transforms back into an $\alpha$-phase that is misoriented from the parent $\alpha$-phase, forming a $\{11\bar{2}2\}$ twin, as shown in Fig. 1c. Afterwards, the $\omega$-phase at the twin tip and the newly formed twin $\alpha$-phase continue to grow along the $\eta_1$ direction, resulting in two long, straight twin boundaries (Fig. 1d). After this twin-lengthening process, the twin thickens perpendicular to the $K_1$ plane, as indicated by the arrow in Fig. 1e. A careful examination of the twin boundaries reveals that the misorientation is $\sim 65^\circ$ across a common $[1\bar{1}00]_\alpha$ direction, matching the theoretical value of the $\{11\bar{2}2\}$ twin in Ti [4]. Interestingly, we find that the intermediate $\omega$-phase can even exist in the growing $\{11\bar{2}2\}$ twin tip, as encircled in Fig. 1c–f, which awaits experimental confirmation using high-resolution characterization techniques. Notably, the residual $\omega$-phase can serve as an evidence of the actual occurrence of the phase transformation-mediated twinning process, while the real-time dynamic process is ultrafast and difficult to observe. Since the density of defects in our samples is largely determined by the quenching rate, we have conducted another simulation with a slower quenching rate and obtained nanotwinned Ti structure that contains a much lower density of defects. Regardless of the quenching rate or the resulting defect concentration, the $\{11\bar{2}2\}$ twins are always found to form through the same martensitic phase transformations via the intermediate $\omega$-phase.

As shown in the inset of Fig. 1b, the close-up view of the intermediate phase reveals it as the $\omega$-phase, which is further confirmed by the radial distribution function (RDF). Fig. 1g shows the evolution of the RDF of a group of approximately 639 atoms in the region undergoing the complete twinning process. As expected, RDFs of the parent and twin only show one major peak within a cutoff distance of 4 Å, corresponding to the lattice parameter $a$=2.95 Å of the $\alpha$-phase. In contrast, RDFs of the intermediate states show four peaks within the same cutoff distance, matching those of the $\omega$-phase. In particular, the $\omega$-phase has three very similar nearest-neighbour distances (2.66 Å, 2.82 Å, and 3.01 Å) and a fourth one of 3.87 Å. This is due to the different packing densities in the A-plane and B-plane of its $A1B_2$ structure. Obviously, the gradual change in the RDF—from $\alpha$-like to $\omega$-like, then back to $\alpha$-like once again-confirms this new $\{11\bar{2}2\}$ twinning mechanism through reversible $\alpha \rightarrow \omega \rightarrow \alpha$ phase transformations.

To quantify the energy barrier of this phase transformation-mediated twinning mechanism, the average potential energy of the same group of atoms is shown in Fig. 1h. The structure shows the first energy jump along with the partial $\alpha \rightarrow \omega$ phase transformation and the second energy jump along with the complete $\alpha \rightarrow \omega$ phase transformation. Then, The structure remains in the $\omega$-phase until the energy peak, followed by an abrupt energy drop due to the activation of the reverse $\omega \rightarrow \alpha$ phase transformation. Afterwards, the potential energy keeps decreasing until the intermediate $\omega$-phase is completely consumed by the newly formed twin $\alpha$-phase. As shown in Fig. 1h, the phase transformation-mediated twinning mechanism for the $\{11\bar{2}2\}$ twin has an approximate energy barrier of $\Delta E = 8.9$ meV/atom.

Based on the above discussions, the $\alpha \rightarrow \omega \rightarrow \alpha$ transformation observed in our MD simulations is rooted in the applied elastic strain and the energy of different phases. First, the applied loading continuously increases the strain in the parent $\alpha$-phase. Thus, the energy of the parent $\alpha$-phase continuously increases until it surpasses the energy of the $\omega$-phase, which leads to the forward $\alpha \rightarrow \omega$ transformation. Then, as we further apply loading to the sample, the strain in the $\omega$-phase keeps rising until it exceeds the energy of the twin $\alpha$-phase, which eventually triggers the reverse $\omega \rightarrow \alpha$ transformation and thus completes the twinning process. Moreover, as calculated from the MEAM potential used in our work, the energy of the $\omega$-phase is only slightly (5 meV/atom) lower than the $\alpha$-phase, which is much lower than the energy difference (110 meV/atom) between the $\alpha$-phase and the $\beta$-phase. It is thus not surprising to find that both forward $\alpha \rightarrow \omega$ and reverse $\omega \rightarrow \alpha$ transformations can occur in our deformation simulation, in which the elastic energy caused by the external loading can well surpass this small energy barrier.

Up to this point, it is important to emphasize that both the forward $\alpha \rightarrow \omega$ and the reverse $\omega \rightarrow \alpha$ transformations follow strict orientation relation. Therefore, the $\{11\bar{2}2\}$ twin is not a coincidence but results from those crystallographic relations. A rigorous trac-

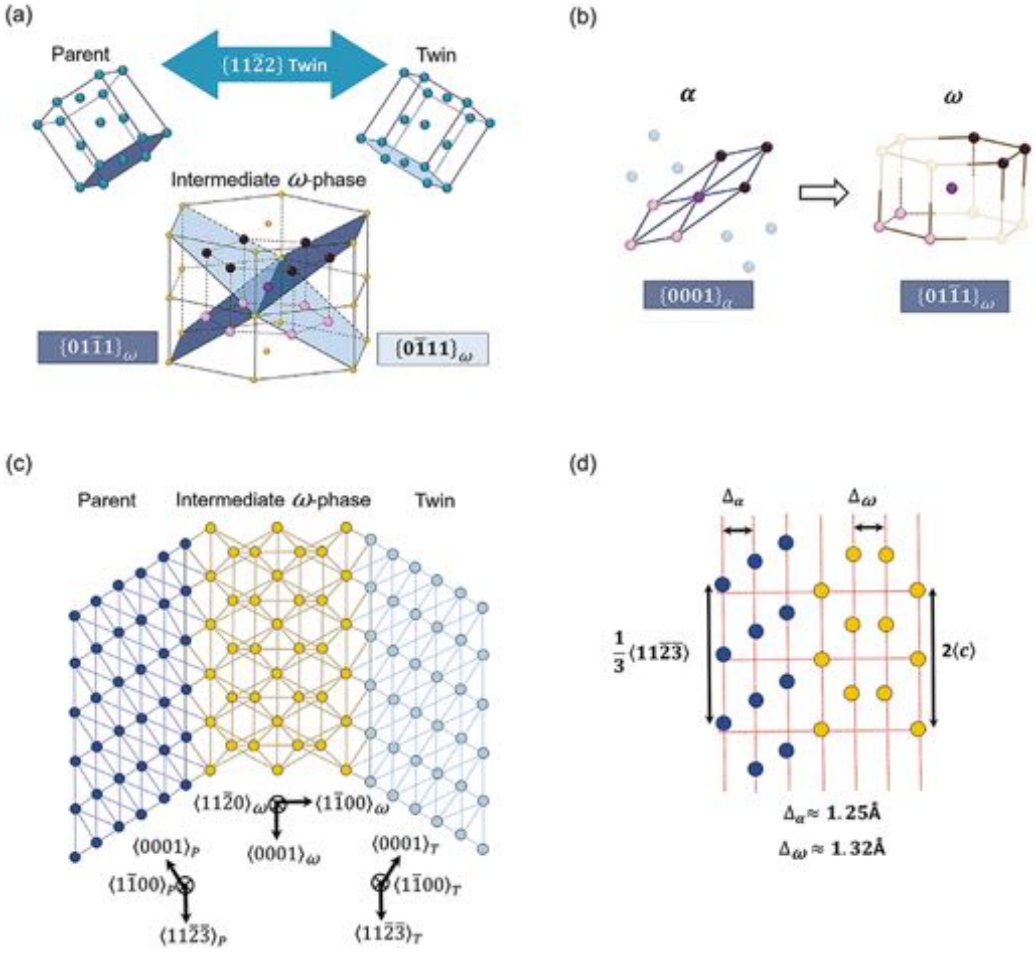


**Fig. 2.** (a) The orientation relation of the phase transformation-mediated twin mechanism and (c) its projection along $[1\bar{1}00]_\alpha$ ($[11\bar{2}0]_\omega$). (b) The atomic evolution during the $\alpha \rightarrow \omega$ transformation: the seven highlighted atoms in the same basal plane of the parent $\alpha$-phase transform into the seven atoms in a corrugated $\{01\bar{1}1\}_\omega$ plane in the intermediate $\omega$-phase. The seven atoms are highlighted by different colors: three black atoms from the top B-plane of the $A1B_2$ structure of the $\omega$-phase, one purple atom from the middle A-plane, and three pink atoms from the bottom B-plane. (d) The $\{1\bar{1}00\}_\alpha$ planes and the $\{11\bar{2}0\}_\omega$ planes have similar atomic arrangement. The subscript "P" and "T" represent the parent and twin, respectively. (For interpretation of the references to color in this figure legend, the reader is referred to the web version of this article.)

ing of the microstructure evolution in our MD simulation reveals that both the forward and reverse phase transformations follow the well-known orientation relation [31] of $(0001)_\alpha \parallel (01\bar{1}1)_\omega$ and $[11\bar{2}0]_\alpha \parallel [\bar{1}011]_\omega$, as schematically shown in Fig. 2a. In particular, a group of atoms are traced in our MD simulations to demonstrate the phase transformation atomistically. As shown in Fig. 2b, seven atoms in one basal plane of the parent $\alpha$-phase, which form a regular hexagon around a central atom, transform into the seven atoms in a corrugated $\{01\bar{1}1\}_\omega$ plane in the intermediate $\omega$-phase during the forward $\alpha \rightarrow \omega$ phase transformation. As expected, the reverse process is found for the reverse $\omega \rightarrow \alpha$ phase transformation.

As highlighted in the $\omega$-unit cell in Fig. 2a, one $\{01\bar{1}1\}_\omega$ plane transforms from the basal plane of the parent $\alpha$-phase, while the other $\{01\bar{1}1\}_\omega$ plane transforms into the basal plane of the twin $\alpha$-phase. It should be noted that this twin formation process is possible and feasible because the angle between the two $\{01\bar{1}1\}_\omega$ planes (63°) is very close to the misorientation angle of the $\{11\bar{2}2\}$ twin (65°). This causes a relatively small lattice distortion and, thus, a small energy barrier for the twinning process (8.9 meV/atom).

Besides the commonly-referred direction correspondence $[11\bar{2}0]_\alpha \parallel [\bar{1}011]_\omega$, another direction correspondence, $[1\bar{1}00]_\alpha \parallel [11\bar{2}0]_\omega$, also plays an important role in the $\{11\bar{2}2\}$ twin formation process. Fig. 2c further demonstrates the orientation relation of the phase transformation-mediated twin mechanism in the projection along the common zone axis $\langle 1\bar{1}00\rangle_\alpha$ of the $\{11\bar{2}2\}_\alpha$ twin, which is also the $\langle 11\bar{2}0\rangle_\omega$ direction. In other words, the twin formation process follows a direction correspondence of

$$\text{Parent } \langle 1\bar{1}00\rangle_\alpha \parallel \text{Intermediate } \langle 11\bar{2}0\rangle_\omega \parallel \text{Twin } \langle 1\bar{1}00\rangle_\alpha. \quad (1)$$

As shown in Fig. 2c, the intermediate $\omega$-phase can be sandwiched between the two $\alpha$-phases coherently. The crystallographical origin of this coherency is that the basal planes of the parent and twin $\alpha$-phases—which are symmetric with respect to the $\{11\bar{2}2\}_\alpha$ plane—correspond to the two crystallographically-equivalent $\{01\bar{1}1\}_\omega$ planes that are symmetric with respect to the $\{1\bar{1}00\}_\omega$ plane. In other words, the twin formation process follows a plane correspondence of

$$\text{Parent } \left\{11\bar{2}2\right\}_\alpha \parallel \text{Intermediate } \left\{1\bar{1}00\right\}_\omega \parallel \text{Twin } \left\{11\bar{2}2\right\}_\alpha. \quad (2)$$

Moreover, the $\{1\bar{1}00\}_\alpha$ planes and the $\{11\bar{2}0\}_\omega$ planes have similar atomic arrangement, as shown in Fig. 2d. The interplanar distance of $\{11\bar{2}2\}_\alpha$ planes (1.25 Å) is close to that of the $\{1\bar{1}00\}_\omega$ planes (1.32 Å), and the length of $1/3[11\bar{2}3]_\alpha = 5.52$ Å is the close to the length of $2c = 5.64$ Å of the $\omega$-phase. As shown in Fig. 2a

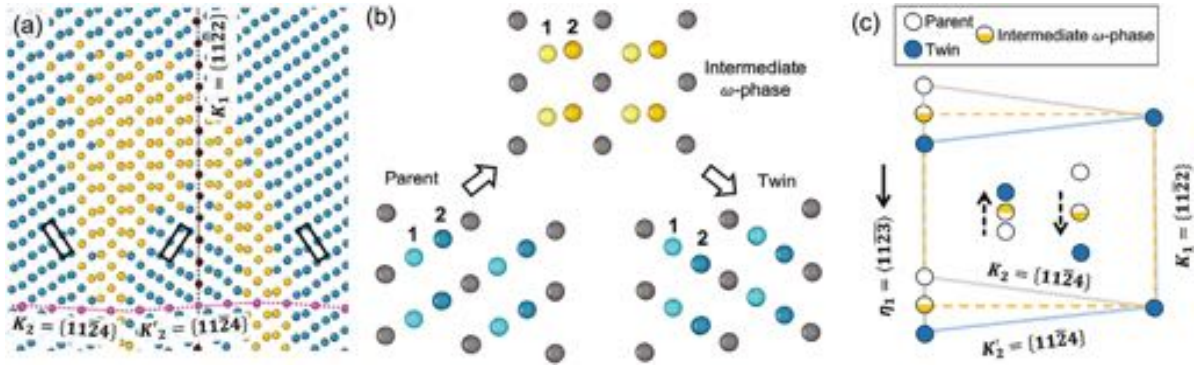


**Fig. 3.** The identification of the twinning mode in our MD simulation. (a) The conjugate twinning plane of the $\{11\bar{2}2\}$ twin is traced in pink and identified as $K_2 = \{11\bar{2}4\}_\alpha$, which transforms into the $\{0001\}_\omega$ plane in the intermediate $\omega$-phase. (b) The evolution of a small group of atoms during the $\{11\bar{2}2\}$ twin formation process in our MD simulation. The atoms corresponding to the A-plane atoms in the $\omega$-phase are colored in gray. The atoms in the other two $K_1$ planes are colored in different shades to clearly show the atom movements during the twinning process. (c) Schematic showing the shear (black arrow) and shuffle (dotted arrows) in our phase transformation-mediated twinning mechanism with an exaggerated $\{11\bar{2}2\}\langle 11\bar{2}3\rangle$ direction (25% larger) to show atom movements more clearly.

and c, the parent and twin $\alpha$-phases are crystallographically equivalent with respect to the intermediate $\omega$-phase. However, the direction of applied loading prefers the twin $\alpha$-phase over the parent one, as evidenced by the energy drop upon the reverse transformation in Fig. 1h. As such, the favorable pathway for accommodating the applied loading is parent $\alpha \rightarrow \omega \rightarrow$twin $\alpha$ phase transformation.

So far, we have demonstrated the complete $\{11\bar{2}2\}$ twinning process observed in our MD simulations, revealing the critical role of the intermediate $\omega$-phase. In the classical twinning theory, Crocker and Bevis identified the $\{11\bar{2}2\}\langle 11\bar{2}3\rangle$ twin observed in experiments as a contraction twin for Ti, which has the second undistorted plane $K_2 = \{11\bar{2}4\}$ and a shear $s = 0.219$ [4]. Recently, Cayron [32] and Gao et al. [33] independently reported a low-shear $\{11\bar{2}2\}\langle 11\bar{2}3\rangle$ twinning mode in Ti, an extension twin with $K_2 = \{11\bar{2}6\}$ and a smaller shear $s = 0.152$ than in the classical twinning theory [4]. Specifically, Gao et al. derived the $\{11\bar{2}2\}$ extension twin using the well-known transformation matrices of hcp→bcc and bcc→hcp phase transformations [33]. Therefore, it is imperative to examine the $K_2$ plane in our phase transformation-mediated twinning mechanism for $\{11\bar{2}2\}$ twin in Ti, which will unambiguously distinguish between different twinning modes with the identical $K_1$ plane [5].

First, we trace a $\{11\bar{2}4\}_\alpha$ plane in the parent $\alpha$-phase during the reversible $\alpha \rightarrow \omega \rightarrow \alpha$ phase transformations. As shown in Fig. 3a, the $\{11\bar{2}4\}_\alpha$ plane first transforms into the $\{0001\}_\omega$ plane in the intermediate $\omega$-phase, and then back into a $\{11\bar{2}4\}_\alpha$ plane in the twin $\alpha$-phase, revealing that our twinning mechanism predicts the same $K_2$ plane and thus the same shear as in the classical twinning theory [4]. Moreover, the $\langle c\rangle$-axis direction of the parent $\alpha$-phase is traced and found to contract in response to z-axis compression, which is equivalent to a $\langle c\rangle$-axis compression. In other words, the $\{11\bar{2}2\}$ twin reported in this paper is a contraction twin with $K_2 = \{11\bar{2}4\}$ and $s = 0.219$. Still, we emphasize that our mechanism recognizes the $\omega$-phase as an intermediate state, while the classical theory misses this dynamical detail.

To further examine the atom movements in the phase transformation-mediated twinning mechanism, a small group of atoms are traced in our MD simulations, and their atom movements are shown in Fig. 3b. Notably, the gray $K_1$ planes undergo a homogeneous shear along the $\eta_1 = \langle 11\bar{2}3\rangle$ direction. Meanwhile, atoms 1 and 2 in the other two $K_1$ planes are within the basal plane of the parent $\alpha$-phase initially; then, they transform into the two atoms in the B-plane of the intermediate $\omega$-phase; finally, they become part of the basal plane of the twin $\alpha$-phase. As a result, the net effect of the above process is that these two atoms shuffle in the opposite $\eta_1$ directions. This twining process is further shown in Fig. 3c, demonstrating that the parent lattice is sheared along the $\eta_1$ direction into the twin lattice, with the $\omega$-lattice as an intermediate state. Our mechanism of $\{11\bar{2}2\}\langle 11\bar{2}3\rangle$ contraction twin agrees with the classical twinning theory in the shuffle and shear [4], but our mechanism also captures the previously undiscovered and critical role of the intermediate $\omega$-phase.

Last but not least, the $\omega$-phase can serve as the intermediate state of the $\{11\bar{2}2\}\langle 11\bar{2}3\rangle$ contraction twin due to its crystallography: the atom structure in the $\omega$-phase is approximately the average of those in the parent and in the twin $\alpha$-phases, as displayed in Fig. 3c. It should also be noted that the $\omega$-unit cell in Fig. 3a is distorted due to the small difference in the interplanar distance between the $\alpha$-phase and the $\omega$-phase, as discussed in Fig. 2d. More detailed lattice distortion and atomic shuffles during the reversible phase transformation are currently under investigation using theoretical and density-functional theory calculations.

To conclude, we have demonstrated the formation of $\{11\bar{2}2\}$ contraction twins in Ti through a non-conventional phase transformation process. In particular, a perfect $\{11\bar{2}2\}$ contraction twin can be formed by an initial transformation from the parent $\alpha$-phase into an intermediate $\omega$-phase, followed by the reverse transformation into a twin $\alpha$-phase. This phase transformation-mediated twinning process, though sharing the same net shear, shuffle, and $K_2 = \{11\bar{2}4\}_\alpha$ plane with the classical twinning theory, reveals the critical role of $\omega$-phase in the twinning process. In addition, we find that a small amount of $\omega$-phase can still exist in the twin tip and coherent twin boundary during the twin-lengthening and twin-thickening processes. This can serve as a trace of the phase transformation-mediated twinning process and can possibly be captured by high-resolution characterization techniques. Furthermore, we note that the reversible phase transformations do not generate an $\alpha$-phase with random orientation, but, rather, follow a strict orientation relation that leads to a $\{11\bar{2}2\}$ twin. Specifically, the phase transformations follow parent $\langle 1\bar{1}00\rangle_\alpha \parallel$ intermediate $\langle 11\bar{2}0\rangle_\omega \parallel$ twin $\langle 1\bar{1}00\rangle_\alpha$ and parent $\{11\bar{2}2\}_\alpha \parallel$ intermediate $\{1\bar{1}00\}_\omega \parallel$ twin $\{11\bar{2}2\}_\alpha$. Our mechanism, emphasizing the evanescent intermediate state of the $\omega$-phase, greatly enhances the classical twinning theory for $\{11\bar{2}2\}$ twins, advancing the understanding of the twinning process in Ti and its alloys, and very likely in other hcp metals. Finally, we note that the critical role of the $\omega$-phase as an intermediate state of the $\{11\bar{2}2\}$ twinning process suggests the opportunity of controlling the twinning process and eventually the related mechanical properties by engineering the properties of the $\omega$-phase. This could greatly diversify current strategies for improving the ductility of Ti and its alloys.

## Declaration of Competing Interest

The authors declare that they have no known competing financial interests or personal relationships that could have appeared to influence the work reported in this paper.

## Acknowledgments

This work was supported by the National Science Foundation (Grant no. #1953300). The authors would like to acknowledge the support of Research & Innovation and the Office of Information Technology at the University of Nevada, Reno for computing time on the Pronghorn High-Performance Computing Cluster.

## References

[1] I.J. Polmear, Mater. Trans. JIM 37 (1) (1996) 12–31.
[2] W.D. Brewer, R.K. Bird, T.A. Wallace, Mater. Sci. Eng.: A 243 (1–2) (1998) 299–304.
[3] R. Schutz, H. Watkins, Mater. Sci. Eng.: A 243 (1) (1998) 305–315.
[4] A. Crocker, M. Bevis, in: R. Jaffee, N. Promisel (Eds.), The Science, Technology and Application of Titanium, Pergamon, 1970, pp. 453–458.
[5] J.W. Christian, S. Mahajan, Prog. Mater. Sci. 39 (1-2) (1995) 1–157.
[6] N.E. Paton, W. Backofen, Metall. Trans. 1 (10) (1970) 2839–2847.
[7] A. Akhtar, J. Nucl. Mater. 47 (1) (1973) 79–86.
[8] E. Rapperport, Acta Metall. 7 (4) (1959) 254–260.
[9] E.J. Rapperport, C.S. Hartley, Trans Metall Soc AIME 218 (1960) 869–876.
[10] H.S. Rosenbaum, R.E. Reed-Hill, J.P. Hirth, H.C. Rogers, in: Deformation Twinning, Gordon and Breach, New York, 1964, pp. 43–76.
[11] A. Serra, D. Bacon, Philos. Mag. A 54 (6) (1986) 793–804.
[12] A. Serra, D. Bacon, Mater. Sci. Eng.: A 400 (2005) 496–498.
[13] J. Morris, Y. Ye, K. Ho, C.T. Chan, M. Yoo, Philos. Mag. Lett. 69 (4) (1994) 189–195.
[14] B. Li, H. El Kadiri, M. Horstemeyer, Philos. Mag. 92 (8) (2012) 1006–1022.
[15] A. Ostapovets, A. Sheikh-Ali, Philos. Mag. 98 (36) (2018) 3235–3246.
[16] S. Rawat, N. Mitra, Comput. Mater. Sci. 141 (2018) 19–29.
[17] J. Ombogo, A.H. Zahiri, T. Ma, L. Cao, Metals 10 (8) (2020) 1030.
[18] B. Li, E. Ma, Phys. Rev. Lett. 103 (3) (2009) 035503.
[19] H.A. Khater, A. Serra, R.C. Pond, Philos. Mag. 93 (10-12) (2013) 1279–1298.
[20] S. Plimpton, J. Comput. Phys. 117 (1995) 1–19.
[21] R.G. Hennig, T.J. Lenosky, D.R. Trinkle, S.P. Rudin, J.W. Wilkins, Phys. Rev. B 78 (2008) 054121.
[22] A.H. Zahiri, J. Ombogo, T.F. Ma, P. Chakraborty, L. Cao, Transformation-induced plasticity in omega titanium, J. Appl. Phys. 129 (1) (2021) 015105, doi:10.1063/5.0035465.
[23] A.H. Zahiri, P. Chakraborty, Y. Wang, L. Cao, J. Appl. Phys. 126 (7) (2019) 075103.
[24] K.D. Joshi, G. Jyoti, S.C. Gupta, S.K. Sikka, Phys. Rev. B 65 (2002) 052106.
[25] A.L. Kutepov, S.G. Kutepova, Phys. Rev. B 67 (2003) 132102.
[26] D.J. Evans, B.L. Holian, J. Chem. Phys. 83 (8) (1985) 4069–4074.
[27] M. Parrinello, A. Rahman, J. Appl. Phys. 52 (12) (1981) 7182–7190.
[28] A. Stukowski, Model. Simul. Mater. Sci. Eng. 18 (1) (2009) 015012.
[29] D. Faken, H. Jónsson, Comput. Mater. Sci 2 (2) (1994) 279–286.
[30] J.D. Honeycutt, H.C. Andersen, J. Phys. Chem. 91 (19) (1987) 4950–4963.
[31] D. Trinkle, R. Hennig, S. Srinivasan, D. Hatch, M. Jones, H. Stokes, R. Albers, J. Wilkins, Phys. Rev. Lett. 91 (2) (2003) 025701.
[32] C. Cayron, Acta Crystallogr. Sect. A 74 (1) (2018) 44–53.
[33] Y. Gao, J.-H. Ke, B. Mao, Y. Liao, Y. Zheng, L.K. Aagesen, Phys. Rev. Mater. 4 (7) (2020) 070601.